JGR Atmospheres

RESEARCH ARTICLE
10.1029/2025JD044655

Increasing Temporal Variability of Global Tropical Cyclone Near-Storm Rainfall Under Global Warming: Insights From CMIP6 HighResMIP Simulations

Jianan Chen[1], Yanzhen Kang[2], Ralf Toumi[3], Lujia Zhang[4], Mengqian Lu[4,5], Xiaoming Shi[6,7], and Dazhi Xi[1]

[1]Department of Earth and Planetary Sciences, University of Hong Kong, Hong Kong, China, [2]College of Atmospheric and Oceanic Sciences, National University of Defense Technology, Changsha, China, [3]Department of Physics, Imperial College London, London, UK, [4]Department of Civil and Environmental Engineering, Hong Kong University of Science and Technology, Hong Kong, China, [5]Otto Poon Centre for Climate Resilience and Sustainability, World Sustainable Development Institute, Hong Kong University of Science and Technology, Hong Kong, China, [6]Division of Environment and Sustainability, Hong Kong University of Science and Technology, Hong Kong, China, [7]Center for Ocean Research in Hong Kong and Macau, Hong Kong University of Science and Technology, Hong Kong, China

Abstract Tropical cyclone (TC) rainfall poses a significant threat to coastal regions, particularly in the near-storm region, where the inner core's strongest convection occurs. Temporal variability in the near-storm rainfall rate over a TC's lifetime, including rapid increases and decreases in rainfall rate, impacts forecast accuracy and hazard preparedness. Using multiple HighResMIP CMIP6 simulations under the SSP5-8.5 scenario, we find that near-storm rainfall rate temporal variability increases under pronounced anthropogenic warming, driven primarily by elevated atmospheric moisture. Analysis of relative rainfall rate changes suggests that this heightened variability aligns with rising near-storm rainfall rate trends. These findings have critical implications for coastal communities, highlighting not only the increased risk of near-storm rainfall but also the rapid intensification or decline of these rainfall events.

Plain Language Summary Tropical cyclones, also known as hurricanes or typhoons, bring heavy rainfall that can cause flooding in coastal areas. Accurately predicting these rainfall patterns is essential for keeping people safe. Our study uses advanced climate models (HighResMIP CMIP6, SSP5-8.5 scenario) to compare rainfall in today's climate with that in a future warmer climate. We found that rainfall near a storm's center will become more unpredictable, with more frequent sudden increases and decreases in rainfall intensity. This is mainly because warmer air can hold more moisture, leading to more variable rainfall. These findings highlight increased flood risks and challenges for forecasting, urging coastal communities to prepare for more unpredictable and intense rainfall events.

Key Points:

- Tropical cyclone near-storm rainfall rate temporal variability, including rapid increase and rapid decrease events, increases under warming
- The increased rainfall rate temporal variability is driven primarily by increased atmospheric moisture
- Rising tropical cyclone near-storm rainfall rate likely drives greater temporal variability

Supporting Information:

Supporting Information may be found in the online version of this article.

Correspondence to:

D. Xi,
dazhixi@hku.hk

Citation:

Chen, J., Kang, Y., Toumi, R., Zhang, L., Lu, M., Shi, X., & Xi, D. (2025). Increasing temporal variability of global tropical cyclone near-storm rainfall under global warming: Insights from CMIP6 HighResMIP simulations. *Journal of Geophysical Research: Atmospheres*, *130*, e2025JD044655. https://doi.org/10.1029/2025JD044655

Received 18 JUN 2025
Accepted 30 OCT 2025

Author Contributions:

Conceptualization: Jianan Chen, Yanzhen Kang
Formal analysis: Jianan Chen, Yanzhen Kang, Ralf Toumi, Dazhi Xi
Funding acquisition: Ralf Toumi, Mengqian Lu, Xiaoming Shi, Dazhi Xi
Investigation: Jianan Chen, Ralf Toumi, Dazhi Xi
Methodology: Jianan Chen, Yanzhen Kang, Ralf Toumi, Dazhi Xi
Project administration: Dazhi Xi
Resources: Ralf Toumi, Mengqian Lu, Dazhi Xi
Software: Jianan Chen, Yanzhen Kang, Lujia Zhang
Supervision: Ralf Toumi, Dazhi Xi
Validation: Jianan Chen, Ralf Toumi, Dazhi Xi
Visualization: Jianan Chen
Writing – original draft: Jianan Chen

1. Introduction

Tropical cyclones (TCs) are among the most devastating natural hazards, characterized by intense winds and torrential rainfall that trigger floods, landslides, and extensive infrastructure damage in coastal regions (Knutson et al., 2020; Shi et al., 2024). Near-storm TC rainfall—precipitation within approximately 100 km of the storm center—is particularly destructive, often leading to extreme flooding events (Liu et al., 2019). The near-storm region, encompassing the eyewall and inner rainbands, exhibits the most intense convective activities, often corresponding to the "inner core" (e.g., Tu et al., 2021). Its potential for rapid rainfall accumulation significantly amplifies societal risks, particularly flooding, making it a critical focus.

The temporal variability of TC near-storm rainfall—marked by rapid increases or decreases in rainfall rates (RR) over short periods—further heightens its importance for flood risk and disaster preparedness (Deng et al., 2025). While rapid intensification (RI) of TC wind speed is a well-established metric for wind-related hazards (Fischer et al., 2019; Y. Li et al., 2021; X. Wang & Jiang, 2021), the RI of near-storm rainfall remains underexplored (Deng et al., 2025). Sudden rainfall surges can significantly amplify freshwater flooding and landslides, overwhelming drainage systems, intensifying inland flooding, and complicating disaster response in vulnerable coastal communities (Deng et al., 2025; Lockwood et al., 2024). This underscores the urgent need for further investigation into rainfall RI to enhance preparedness and mitigate impacts. Global warming, driven by rising greenhouse gas

Writing – review & editing: Jianan Chen, Yanzhen Kang, Ralf Toumi, Lujia Zhang, Xiaoming Shi, Dazhi Xi

concentrations, alters atmospheric conditions in ways that influence TC near-storm rainfall. Warmer sea surface temperatures (SST) and increased atmospheric moisture, governed by the Clausius-Clapeyron relationship, enhance TC convection, leading to intensified TC activity (e.g., Kim et al., 2022; Knutson et al., 2020). The combined effect of stronger TC intensity and higher moisture content amplifies this increase beyond what moisture alone would dictate via Clausius-Clapeyron scaling (Liu et al., 2019). However, increased atmospheric stability under warming has been linked to reductions in near-storm rainfall, introducing complexity to these trends (e.g., Tu et al., 2021).

Investigating these complex TC rainfall patterns under warming relies heavily on two primary modeling approaches: global climate models (GCMs) and cloud-resolving models (CRMs). GCMs, with typical resolutions around 100 km, simulate global TCs over extended periods and large scales but struggle to resolve fine-scale rainfall structures like rainbands and near-storm dynamics (e.g., Patricola & Wehner, 2018; Stansfield & Rasmussen, 2025; Xi et al., 2022; Yang & Toumi, 2025). Despite this, they consistently project increases in near-storm rainfall under warming (Knutson et al., 2020), a finding echoed by higher-resolution CRMs that explicitly capture inner core convective processes (Stansfield & Rasmussen, 2025; Xi et al., 2022; Yang & Toumi, 2025). Both modeling communities thus agree that future TC inner core rainfall will rise, driven by enhanced moisture availability and storm intensity (e.g., Knutson et al., 2020; Patricola & Wehner, 2018; Yang & Toumi, 2025). In contrast, observational data from 1998 to 2019 reveal a global decrease in TC inner core rainfall (Tu et al., 2021), with its temporal variability declining by $1.74 \pm 0.57\%$ and $2.23 \pm 0.55\%$ per decade (Deng et al., 2025). This discrepancy with model projections may stem from natural variability or anthropogenic factors, such as aerosols, obscuring warming signals during the modest temperature rise (0.5°C) observed over this period (Stansfield & Rasmussen, 2025). While CRMs effectively capture mean TC precipitation characteristics (Xi et al., 2022), their computational demands limit their use for large-ensemble studies of temporal variability. Consequently, GCMs remain vital for long-term trend analysis despite their resolution constraints. To address the resolution limitations in GCM simulations and ensure robustness, we investigate near-storm rainfall variability using multiple radii (100–300 km) from the TC center.

This study investigates the temporal variability of global TC near-storm rainfall under warming, including both absolute and relative changes in rainfall rate. Validated against multiple HighResMIP models, our analysis reveals increasing temporal variability under substantial warming, contrasting with observed trends toward reduced temporal variability. These findings highlight critical implications for flood risk and adaptation strategies in a warming world.

2. Method

2.1. Data

The primary data used in this study is from the Coupled Model Intercomparison Project Phase 6 (CMIP6) HighResMIP "highresSST-future" (atmosphere-only) experiment, utilizing the Meteorological Research Institute (MRI) Atmospheric General Circulation Model version 3.2 with a 25-km horizontal grid resolution (Mizuta et al., 2019). This data set covers the period from 2015 to 2099 under the SSP5-8.5 scenario, providing daily outputs that facilitate a continuous, long-term analysis of TC behavior—a distinctive advantage among HighResMIP products. The MRI model excels at simulating intense TCs, including Category 4–5 storms (J. Roberts et al., 2020), making it an ideal tool for investigating the impacts of climate change on TC rainfall and intensity. As one of the few global circulation models capable of resolving the strongest TCs, it provides critical insights into potential shifts in TC characteristics driven by a warming climate. TCs are identified and tracked using the TempestExtremes software package (Ullrich et al., 2021). This algorithm detects TCs by locating a sea-level pressure minimum that coincides with an upper-level warm core, with comprehensive tracking metrics outlined in Chen et al. (2025). Although the MRI data set includes only a single ensemble member, its high resolution and extended simulation period (2015–2099)—exceeding the typical 2015–2050 range of HighResMIP products—make it the primary focus of this analysis. The observation rainfall data is from the IMERG Final Precipitation L3 Half Hourly $0.1° \times 0.1°$ V07 (Huffman et al., 2023).

To validate the MRI model results, we incorporate two additional high-resolution models: EC-Earth3P-HR (Haarsma et al., 2020) and HadGEM3-GC31-HM (Roberts et al., 2019). For EC-Earth3P-HR, we use the "highresSST-future" (atmosphere-only) experiment, which isolates atmospheric responses to prescribed SST changes, providing a focused view of atmospheric dynamics. For HadGEM3-GC31-HM, we employ the

"highres-future" (fully coupled) simulation, which captures the integrated climate system response, including ocean-atmosphere feedbacks. Each model provides three ensembles, enhancing statistical robustness, and both operate at a coarser 50-km grid resolution. The two models were selected for their ensemble availability and well-documented cyclone tracks, though their simulations are limited to a shorter period, 2015 to 2050, under the SSP5-8.5 scenario. This combination of atmosphere-only and coupled simulations broadens the scope of our validation effort. Storm tracks in these models are generated using the TempestExtremes and TRACK algorithms, as described in (Roberts, 2019a, 2019b). Both tracking methods yielded consistent results, showing increased TC near-storm RR temporal variability. This study presents results based on the TempestExtremes algorithm (Roberts, 2019a). To ensure a focus on tropical storms, the analysis restricts storm tracks to latitudes between 30°S and 30°N.

2.2. Metrics

TC snapshots are categorized by intensity, derived from 10-m maximum wind speed ($V_{\max,10m}$), into tropical storm (TS) and Categories 1–5 (CAT1–CAT5) based on the Saffir–Simpson Hurricane Wind Scale. Unlike our prior work of Chen et al. (2025), this study includes landfall TCs. Environmental moisture is quantified using monthly total column water vapor (TCW) following Chen et al. (2025). Dry static atmospheric stability (DSAS), as defined by Sharmila and Walsh (2018), is the potential temperature difference between 300 hPa and 900 hPa, expressed as $\theta_{300} - \theta_{900}$. Both DSAS and TCW are computed using their monthly mean values at the TC center. The monthly means, reflecting persistent background conditions, provide a clearer signal of the climatic drivers of rainfall compared to daily conditions influenced by the storm itself (e.g., Chen et al., 2025; Lockwood et al., 2024). Following Liu et al. (2019), we define near-storm rainfall as mean rainfall within 100 km of the TC center, unless otherwise specified, as this region encompasses the eyewall and inner rainbands where the most intense rainfall occurs. The rain rate is from 24-hourly climate model output. To assess robustness across spatial scales, we also analyze near-storm rainfall using radii from 100 to 300 km, with results presented in Section 3.6.

To quantify TC rainfall rate and intensity temporal variability, we calculate the 24-hr change in near-storm RR and maximum surface wind speed ($V_{\max,10m}$) following Deng et al. (2025):

$$\Delta R_{24h} = R_{t+24h} - R_t, \tag{1a}$$

$$\Delta V_{24h} = V_{\max,t+24h} - V_{\max,t}, \tag{1b}$$

where R_t and R_{t+24h} are the near-storm RRs at times t and $t + 24$ hours, and $V_{\max,t}$ and $V_{\max,t+24h}$ are the corresponding 10-m maximum wind speeds. Additionally, we compute the relative change in near-storm rainfall rate, defined as $\Delta R_{24h}/R_t$ to capture the proportional magnitude of rainfall fluctuations relative to the initial rainfall rate. This metric is particularly useful for assessing the magnitude of rapid changes in rainfall relative to baseline conditions, complementing the absolute change ΔR_{24h}. By default, ΔV_{24h} refers to the 10 m wind speed change ($\Delta V_{24h,10m}$, using $V_{\max,10m}$) unless otherwise specified. In Section 3.3, we distinguish between $\Delta V_{24h,10m}$ and $\Delta V_{24h,850hPa}$ (using $V_{\max,850hPa}$) to compare their relationships with near-storm RR change.

Thresholds of rapid increase (RI) and rapid decrease (RD) for RR and intensity are defined using the 95th and 5th percentiles of ΔR_{24h} and ΔV_{24h} for the entire data set. The RR RI events are ΔR_{24h} values exceeding the 95th percentile threshold, and RR RD events are those below the 5th percentile threshold. Similarly, intensity RI and RD events are defined for ΔV_{24h} exceeding the 95th percentile or falling below the 5th percentile, respectively.

3. Results

3.1. Widening in Annual TC 24-hr RR Changes

Contrary to observed decreases in TC near-storm RR temporal variability (Deng et al., 2025), simulations from the MRI model under the CMIP6 HighResMIP "highresSST-future" experiment (2015–2099, SSP5-8.5 scenario) reveal a robust increase in the variability of near-storm rainfall. Figure 1 illustrates the interannual trends in the 95th and 5th percentiles of rain rate changes (ΔR_{24h} in mm/h) for global TCs from 2015 to 2099. The 95th percentile of ΔR_{24h}, representing thresholds for RI of near-storm RR, exhibits a statistically significant positive trend. This trend indicates that the magnitude of rapid rainfall increases intensifies under warming. Conversely, the 5th percentile of ΔR_{24h}, representing thresholds for RD of near-storm RR, shows a significant negative trend.

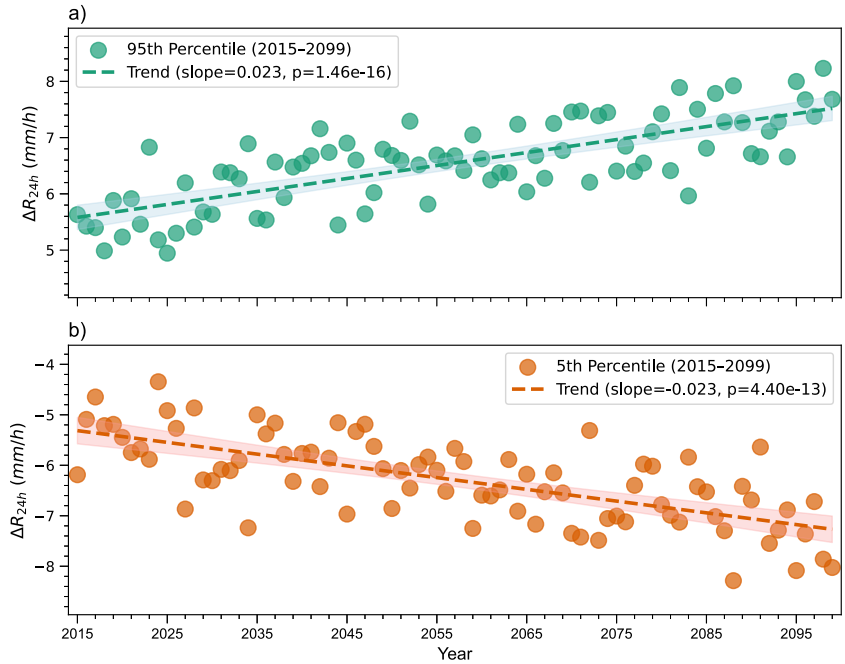

Figure 1. Interannual trends of the 95th and 5th percentiles of 24-hr near-storm rainfall rate changes (ΔR_{24h}, mm/h) for global tropical cyclones from 2015 to 2099. Subplots show trends for: (a) 95th percentile of ΔR_{24h} for near-storm rainfall, (b) 5th percentile of ΔR_{24h} for near-storm rainfall. The shaded area indicates the 95% confidence interval for the regression slope.

This trend suggests that rapid rainfall decreases also become more pronounced. These opposing trends collectively indicate a widening range of near-storm rainfall variability, with both extreme increases and decreases becoming more intense under future warming.

To assess the robustness of these trends across different spatial scales, we analyzed regression slopes of ΔR_{24h} quantiles (5th to 95th percentiles, at 5% intervals) for rainfall within 100, 150, 200, 300, and 500-km radii from the TC center, as shown in Figure 2. The slopes, depicted as solid dots for statistically significant trends ($p \leq 0.05$) and hollow dots for non-significant trends, reveal consistent patterns across most quantiles and radii. For the near-storm RR using the 100 km averaging radius, the 95th percentile slope (0.023 mm/hr/year) and 5th percentile slope (−0.023 mm/hr/year) are highly significant, reflecting strong trends in RI and RD. These trends remain significant for most quantiles, with non-significant trends emerging only near the median (e.g., 45th–50th percentiles, $p > 0.05$). Notably, the magnitude of regression slopes for the 95th percentile of ΔR_{24h} increases with decreasing averaging radius, from 0.0041 mm/hr/year at 500 km ($p \leq 0.01$) to 0.023 mm/hr/year at 100 km. This pattern suggests that rainfall variability is most pronounced closer to the TC center, where higher averaged rainfall rates reflect intensified convective activity within 100 km of the storm center. Similarly, the 5th percentile slopes show stronger negative trends at smaller radii (e.g., −0.023 mm/hr/year at 100 km vs. −0.0020 mm/hr/year at 500 km, $p \leq 0.01$), indicating that rapid rainfall declines are also more extreme near the storm center.

3.2. Increases in TC RR Rapid Changes

To further explore the temporal variability of TC near-storm rainfall under warming, we analyze the interannual trends of RR RI/RD event ratios, as shown in Figure 3. These event ratios, calculated as the number of RR RI or RD events divided by the annual count of TC snapshots, quantify the probability of extreme rainfall variability events. The thresholds for RR RI and RD events are derived from the entire MRI data set from 2015 to 2099, using the 95th and 5th percentiles of ΔR_{24h}, yielding values of 6.592 mm/hr for RI and −6.356 mm/hr for RD, respectively. Over the full period from 2015 to 2099, regression analysis reveals statistically significant increases in the near-storm RR RI ratio (slope: 0.042 per year, $p < 0.01$) and the RR RD ratio (slope: 0.041 per year, $p < 0.01$), with 95% confidence intervals of ±0.0099 and ±0.0107 per year, respectively. To test the sensitivity of thresholds for RR RI and RD events, we also computed RR RI and RD thresholds using only the Present climate (2015–2035), yielding thresholds of 5.844 mm/h for RR RI and −5.730 mm/h for RR RD. The same robust

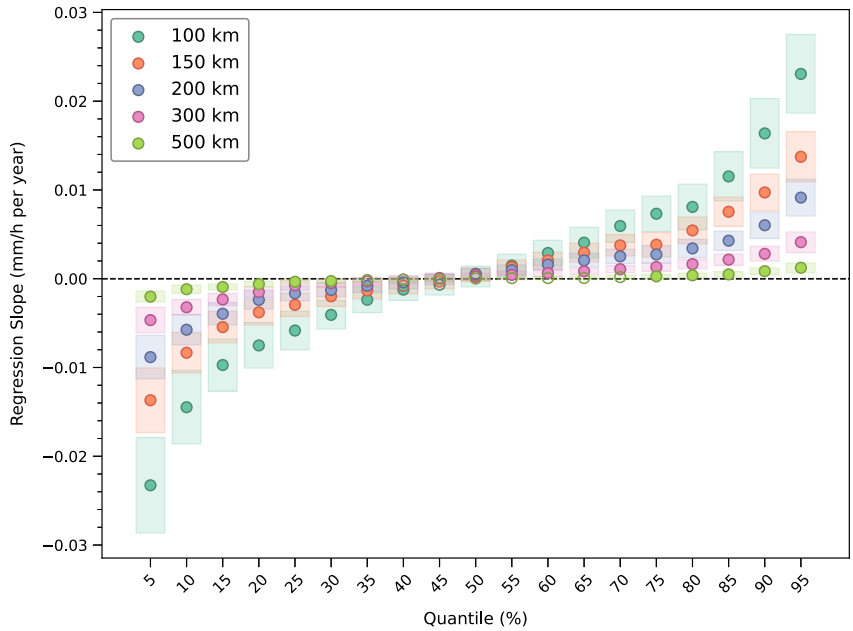

Figure 2. Regression slopes of quantiles of 24-hr near-storm rainfall rate changes within 100, 150, 200, 300, and 500 km radii for global tropical cyclones from 2015 to 2099. Dots represent least squares regression slopes for quantiles from the 5th to 95th percentiles (in 5% intervals). Shaded areas indicate 95% confidence intervals. Solid dots denote statistical significance ($p \leq 0.05$); hollow dots indicate non-significance.

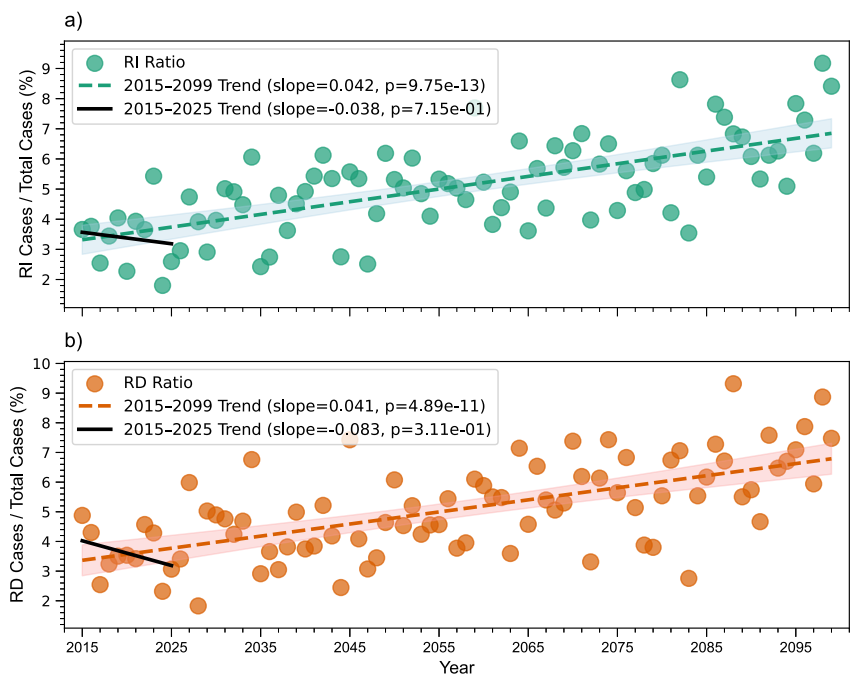

Figure 3. Interannual trends of near-storm rainfall rate (RR) rapid increase (RI) and rapid decrease (RD) event ratios for global tropical cyclones from 2015 to 2099. Event ratios are calculated as the number of RR RI or RR RD snapshots divided by the annual number of TC snapshots. Subplots show: (a) RR RI event ratio, (b) RR RD event ratio, with dashed lines indicating regression trends (2015–2099) and shaded areas representing 95% confidence intervals. Black solid lines denote regression trends for 2015–2025, reflecting short-term trends.

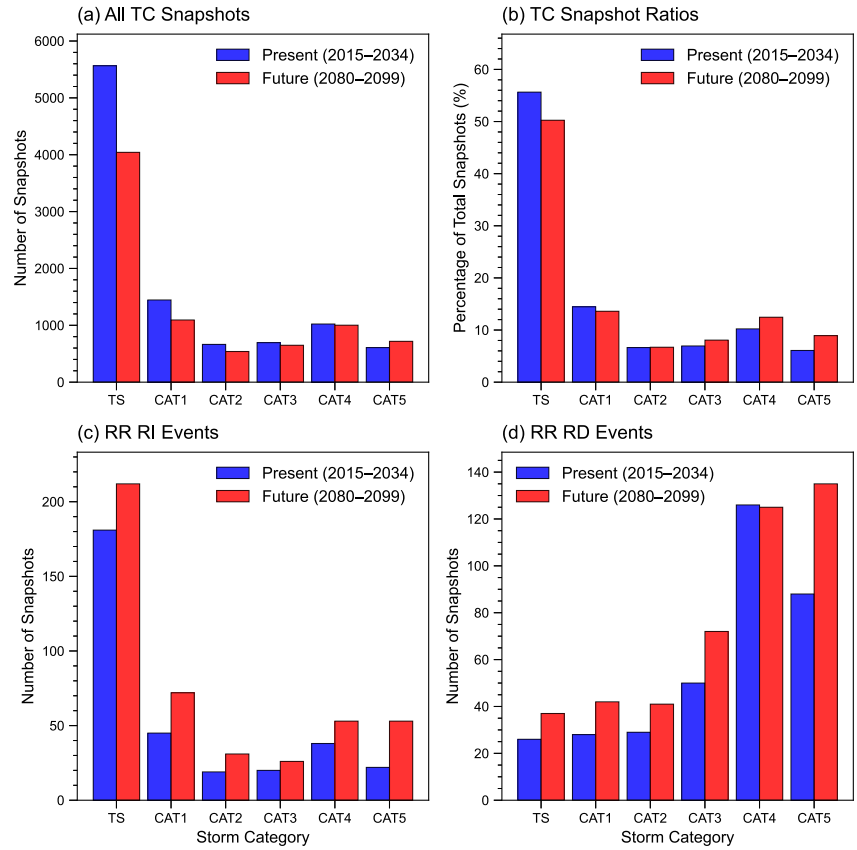

Figure 4. Bar plots showing TC snapshots by storm category (TS, CAT1–CAT5) for Present (2015–2034) and Future climates (2080–2099). (a) Raw counts of TC snapshots. (b) Ratios (%) of TC snapshots per category relative to total snapshots. (c) Counts of rainfall rate rapid increase snapshots. (d) Counts of rainfall rate rapid decrease snapshots.

increases (RR RI: slope: 0.056 per year, $p < 0.01$; RR RD: slope: 0.048 per year, $p < 0.01$) is found (see Figure S1 in Supporting Information S1). These robust trends indicate a consistent, long-term rise in the frequency of extreme rainfall variability events associated with TCs. In contrast, over the shorter period from 2015 to 2025, both ratios exhibit negative trends (RR RI ratio: slope $= -0.038$, $p = 0.715$; RR RD ratio: slope $= -0.083$, $p = 0.311$), though these are not statistically significant (Figure 3). These short-term trends likely arise from natural variability rather than a persistent signal, highlighting the critical role of extended simulations in distinguishing anthropogenic influences from internal natural variability. We emphasize that this study focuses on the response of near-storm rainfall variability to pronounced warming over the full 2015–2099 period, rather than short-term trends or direct comparisons with historical observations.

Despite some projections of a decline in annual TC frequency under global warming (Knutson et al., 2020), complementary metrics—such as RR RI/RD events per TC (Figure S2 in Supporting Information S1) and raw counts of RR RI/RD events (Figure S3 in Supporting Information S1)—also exhibit statistically significant increasing trends over the full period. This consistency across multiple metrics underscores the robustness of the observed increase in the temporal variability of TC rainfall. Such findings imply that, even as TC frequency may decrease, the rainfall dynamics within individual TCs could become more erratic, resulting in more frequent shifts in rainfall intensity or heightened risks of extreme rainfall events.

To assess changes under warming, we analyze RR RI and RD events in the MRI data set across two climate periods: Present (2015–2034) and Future (2080–2099). Figure 4a presents bar plots of TC snapshot counts by storm category (tropical storm, TS; Categories 1–5, CAT1–CAT5) for both periods. Total TC snapshots decrease from 10,001 in the Present climate to 8,044 in the Future climate, a reduction of 19.6%, consistent with projections of declining annual TC frequency under warming (Knutson et al., 2020). The storm category distribution reveals significant shifts in TC intensity. In the Future climate, TS snapshots decrease markedly by 27.4% (from 5,565 to

4,042), while CAT5 snapshots increase by 18.1% (from 608 to 718). This shift toward a higher proportion of intense TCs (CAT4–CAT5, Figures 4a and 4b) aligns with projections of increased TC intensity under warming (Knutson et al., 2020).

The storm category distribution of near-storm RR RI and RR RD events, categorized by initial intensity at the start of the 24-hr period change, is shown in Figures 4b and 4c. The near-storm RR RI events total 325 in the Present climate, with TS contributing 55.7% (181/325), followed by CAT1 (45, 13.8%) and CAT4 (38, 11.7%). The near-storm RR RD events total 347 in the Present climate, predominantly from CAT4–CAT5 (214/347≈61.7%), with CAT4 at 126 (36.3%) and CAT5 at 88 (25.4%). This suggests that rapid near-storm rainfall rate changes occur primarily at opposite ends of the intensity spectrum, with TS driving RR RI events and high-intensity storms (CAT4–CAT5) driving RR RD events. Of note, high-intensity TCs are associated with RR RD, likely due to the strong correlation between near-storm rain rate changes and TC intensity changes. Specifically, high-intensity storms drive rapid decreases in TC intensity, as demonstrated by Ma et al. (2019) and S. Wang et al. (2020). Consequently, physical mechanisms influencing TC intensity RD also affect RR RD, including geographical factors such as TC landfall and environmental factors like high vertical wind shear (VWS) and low relative humidity (RH) (e.g., M. Li & Toumi, 2024). We analyzed environmental VWS and RH at the onset of RR RD and RI events. Environmental RH is computed as the average within a 200–800 km annulus around the TC center, using data from the 700 hPa and 500 hPa pressure levels. Environmental VWS is calculated as the magnitude of the wind vector difference between 850 hPa and 250 hPa, averaged over the same 200–800 km annulus. We found that compared to RR RI, the RR RD are featured by lower-RH and higher-VWS (see Figure S4 in Supporting Information S1), indicating dry, disruptive conditions drive rain rate decreases.

In the Future climate, RR RI events rise to 447 (+37.5%), with TS at 47.4% (212/447) and notable increases in CAT5 (+140.9%, 22 to 53) and CAT1 (+60.0%, 45 to 72). The near-storm RR RD events increase to 452 (+30.3%), with CAT5 rising sharply (+53.4%, 88 to 135) and increases in weaker categories (e.g., TS +42.3%, 26 to 37), but a slight decrease in CAT4 (−0.8%, 126 to 125).

RR RI and RD events are predominantly concentrated in subtropical regions, including the western North Pacific, eastern North Pacific, North Indian Ocean, and Australian basin (Figure S5 in Supporting Information S1). Compared to RR RI events, RR RD events occur more frequently near coastal areas, where landfall disrupts moisture supply and convection. Figure 5 illustrates the latitudinal distribution of these events. RR RI events peak at 17.5° (15–20° bin) with 69 events in the Present climate and 95 in the Future climate, indicating that subtropical regions are primary zones for rapid rainfall increases. RR RD events peak at 22.5° (20–25° bin) with 79 events in the Present climate and 118 in the Future, reflecting a preference for higher latitudes than RR RI events. While RR RI events peak latitudes remain stable across climates, the significant increase in RR RI events and a reduction in RR RI events at low latitudes (5–10°, −5 to −10°) suggest that warming-driven poleward shifts in TC tracks (e.g., Cao et al., 2023, 2024, 2025; T. Li et al., 2010) may enhance the frequency of TCs reaching optimal intensification zones.

3.3. Relationship Between RR Change and Intensity Change

For RR RI events, many TCs begin as tropical storms but intensify to CAT1-CAT5 by the end of the 24-hr period (Figure 4), suggesting a link between RR change ΔR_{24h} and TC intensity change ΔV_{24h}. Our prior work (Chen et al., 2025) suggests that near-storm RR scales better with maximum wind speed at 850 hPa ($V_{max,850hPa}$) than at 10 m ($V_{max,10m}$). Our linear regression analyses confirm this, showing a stronger correlation between near-storm ΔR_{24h} and $\Delta V_{24h,850hPa}$ (ρ = 0.699 Present, 0.7247 Future) compared to $\Delta V_{24h,10m}$ (ρ = 0.621 Present, 0.615 Future) in both Present and Future climate.

In the Present climate, the near-storm ΔR_{24h} increases by 0.47 mm/hr per m/s increase in $\Delta V_{24h,850hPa}$, while in the Future climate, this sensitivity rises to 0.57 mm/hr per m/s, a 22.7% increase, indicating enhanced responsiveness of near-storm rain rate changes to storm intensity changes under warming (Figure 6). The amplified sensitivity of ΔR_{24h} to $\Delta V_{24h,850hPa}$ in the Future climate is likely driven by increased environmental moisture. When TCW is incorporated, ΔR_{24h} exhibits proportionality to the product of $\Delta V_{24h,850hPa}$ and TCW, expressed as $\Delta R_{24h} = \alpha \cdot \Delta V_{24h,850hPa} \cdot \mathrm{TCW}$. This relationship produces nearly consistent scaling, with regression slopes (α) of 0.0095 mm/hr per mm·m/s in the Present climate and 0.0096 mm/hr per mm·m/s in the Future climate, corresponding to a +1.0% difference. Under warming conditions, increased moisture availability (TCW) amplifies

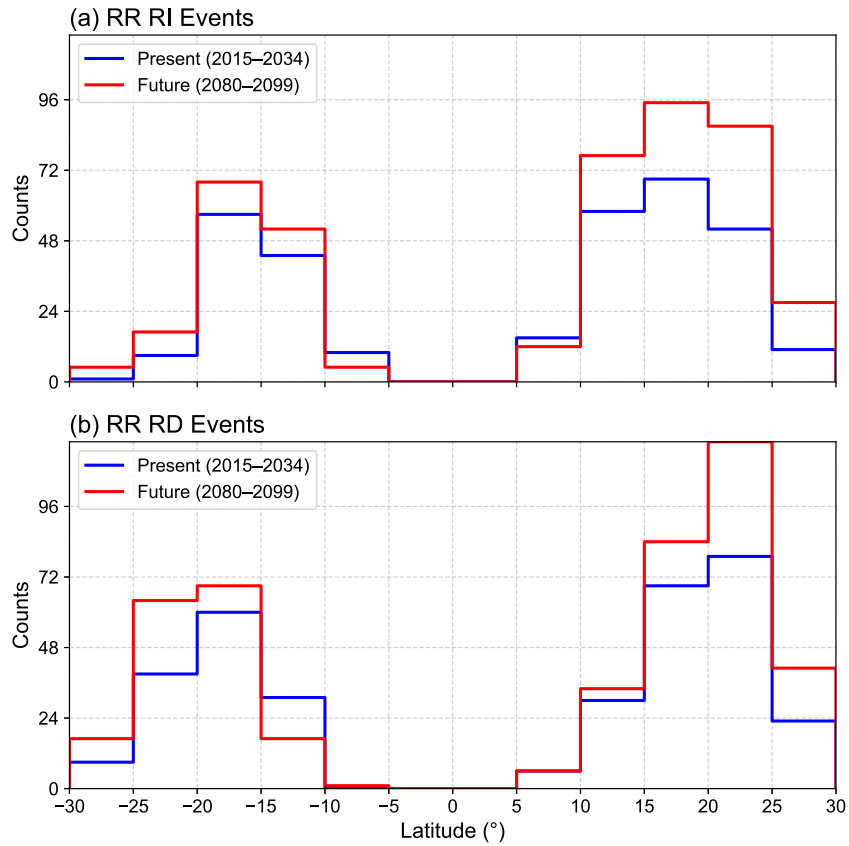

Figure 5. Latitudinal distribution of near storm rain rate RI (a) and RD (b) events for Present (2015–2034) and Future climates (2080–2099).

ΔR_{24h} for a given ΔV_{24h}, leading to enhanced responsiveness of ΔR_{24h} to ΔV_{24h} under warming. When ΔV_{24h} is negative (positive), increased TCW amplifies the magnitude of the negative (positive) ΔR_{24h}, leading to sharper declines (increase) in rainfall rate. Thus, the increased TCW under warming conditions intensifies both positive and negative fluctuations in near storm rainfall, contributing to greater temporal variability, including both rapid decreases and rapid increases. In contrast, Deng et al. (2025) suggested that increased TCW stabilizes temporal rainfall variability by negatively correlating with RD events. Here, we propose that higher TCW enhances intensity-driven RR changes, amplifying both RI and RD events and thus increasing overall variability.

To further elucidate the physical drivers of near-storm RR changes under warming, we analyze the change of ΔR_{24h} for RR RI and RR RD events between Present and Future climate. The stable scaling of ΔR_{24h} with $\mathrm{TCW} \cdot \Delta V_{24h,850hPa}$ across climates implies that variations in ΔR_{24h} are driven by changes in TCW and $\Delta V_{24h,850hPa}$, rather than changes in the scaling itself. To quantify these contributions, we decompose the change in mean ΔR_{24h} for RR RI and RD events as follows:

$$\delta\overline{\Delta R}_{24h,RI} = \left(\alpha \cdot \delta\overline{\Delta V}_{24h,850hPa,RI} \cdot \langle\overline{\mathrm{TCW}}_{RI}\rangle\right) + \left(\alpha \cdot \langle\overline{\Delta V}_{24h,850hPa,RI}\rangle \cdot \delta\overline{\mathrm{TCW}}_{RI}\right), \quad (2)$$

$$\delta\overline{\Delta R}_{24h,RD} = \left(\alpha \cdot \delta\overline{\Delta V}_{24h,850hPa,RD} \cdot \langle\overline{\mathrm{TCW}}_{RD}\rangle\right) + \left(\alpha \cdot \langle\overline{\Delta V}_{24h,850hPa,RD}\rangle \cdot \delta\overline{\mathrm{TCW}}_{RD}\right), \quad (3)$$

where δ denotes the difference between climates, $\langle\cdot\rangle$ represents the mean across climates, the overbar ($\bar{\cdot}$) indicates the average for RD or RI events, and α is assigned a value of 0.0095 mm/h per mm·m/s. The thermodynamic contribution is associated with changes in TCW, while the dynamic contribution is linked to changes in $\Delta V_{24h,850hPa}$.

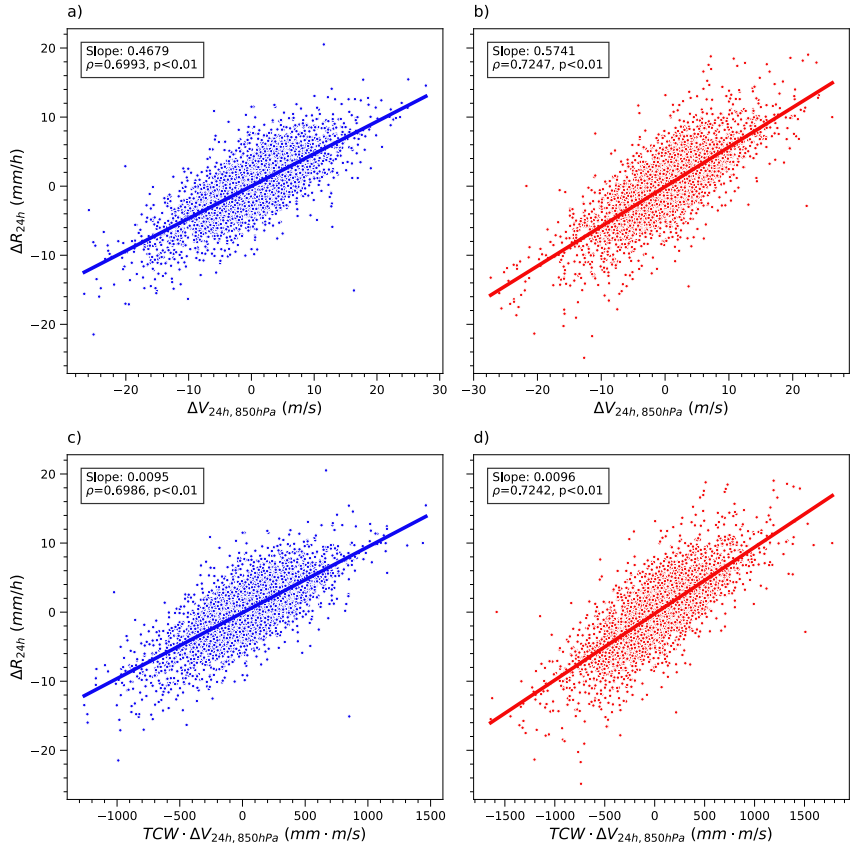

Figure 6. Correlation analysis showing the relationship between 24-hr near-storm rainfall rate change (ΔR_{24h}, mm/h) and TC intensity change ($\Delta V_{24h,850hPa}$, m/s, defined as the change in maximum wind speed at 850 hPa, $V_{max,850hPa}$) (a, b) or the product of total column water vapor and the TC intensity change (TCW · $\Delta V_{24h,850hPa}$, mm·m/s) (c, d). Panels (a, c) represent the Present climate (2015–2034), while panels (b, d) depict the Future climate (2080–2099).

For RR RI events, $\delta\overline{\Delta R}_{24h,RI} = 0.650$ mm/h, with the dynamic contribution given by $\alpha \cdot \delta\overline{\Delta V}_{24h,850hPa,RI} \cdot \langle\overline{TCW}_{RI}\rangle = 0.12$ mm/h and the thermodynamic contribution by $\alpha \cdot \langle\overline{\Delta V}_{24h,850hPa,RI}\rangle \cdot \delta\overline{TCW}_{RI} = 0.68$ mm/h. The sum ($0.12 + 0.68 = 0.80$ mm/h) slightly overestimates $\delta\overline{\Delta R}_{24h,RI} = 0.650$ mm/h, suggesting a good approximation and minor nonlinear effects. The thermodynamic contribution dominates ($|0.68| > |0.12|$), suggesting the increased moisture play a dominant role in amplifying the RR RI under warming. For RR RD events, $\delta\overline{\Delta R}_{24h,RD} = -0.52$ mm/h, with the dynamic contribution given by $\alpha \cdot \delta\overline{\Delta V}_{24h,850hPa,RD} \cdot \langle\overline{TCW}_{RD}\rangle = -0.039$ mm/h and the thermodynamic contribution by $\alpha \cdot \langle\overline{\Delta V}_{24h,850hPa,RD}\rangle \cdot \delta\overline{TCW}_{RD} = -0.61$ mm/h. The thermodynamic contribution dominates ($|-0.61| > |-0.039|$), suggesting the increased moisture play a dominant role in amplifying the RR RD under warming.

The physical mechanisms driving the increase in TC intensity RI under warming conditions have been partially explained from the perspective of more favorable thermodynamic environments (Bhatia et al., 2022). However, the mechanisms underlying the increase in TC intensity RD under warming remain underexplored (S. Wang et al., 2020), despite evidence of their enhancement (Bhatia et al., 2019). A comprehensive understanding of these phenomena requires accurate simulation of both large-scale environmental fields and TC internal dynamics (Bhatia et al., 2022). Environmental factors, such as sea surface temperature, vertical wind shear, and atmospheric humidity, set the large-scale conditions influencing TC intensity changes. However, internal dynamics, including eyewall replacement cycles and vortex interactions, play a critical role in rapid intensity changes (Bhatia et al., 2022). Current climate model simulations, even HighRes CMIP6 simulations used in our study, typically operating at resolutions of tens of kilometers, struggle to resolve TC internal dynamics (Shi et al., 2024). This limitation hinders a comprehensive understanding of RD and RI trends under warming, as models may not fully represent the rapid weakening mechanisms (Bhatia et al., 2022).

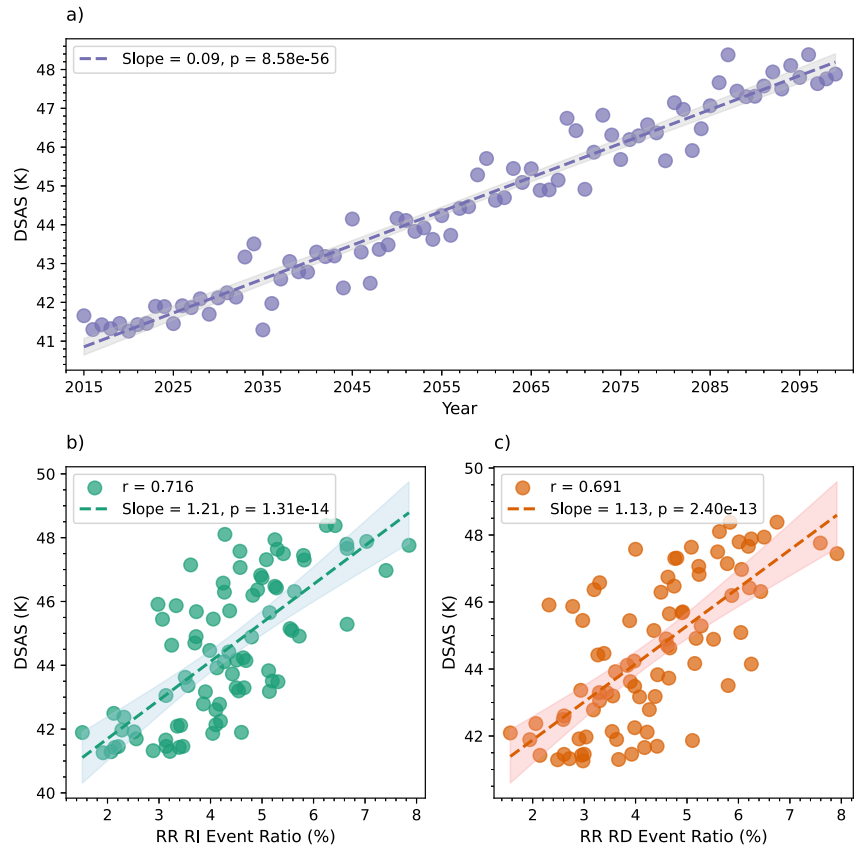

Figure 7. (a) Interannual trends of mean dry static atmospheric stability (DSAS, in k). (b) Annual mean DSAS versus mean near-storm rainfall rate (RR) rapid increase (RI) event ratio (%). (c) Annual mean DSAS versus near-storm RR rapid decrease (RD) event ratio (%). The shaded area indicates the 95% confidence interval for the regression slope.

Given the strong correlation between 24-hr near-storm RR changes and TC intensity changes, we now examine how TC intensity RI and RD events evolve under warming. The TC intensity RI and RD events show slight changes between Present climate and Future climate. TC Intensity RI events (427 Present, 455 Future, +6.6%) and RR RI events (325 Present, 447 Future, +37.5%) show contrasting increase amplitudes under warming, with near-storm RR RI events exhibiting a significantly larger rise. Similarly, TC intensity RD events (416 Present, 407 Future, −2.2%) decrease slightly, while near-storm RR RD events (347 Present, 452 Future, +30.3%) increase substantially. These differences, suggest that increased environmental TCW enhances both RR RI and RR RD more than intensity RI or RD contributes to their respective RR changes under warming. This underscores moisture's role in amplifying rainfall variability compared to the more muted response of intensity events. Of note, despite a modest increase in TC intensity RI events from 427 to 455 (+6.6%) under warming, the annual TC frequency decreases significantly from 74.05 to 59.25 (−20.0%). Consequently, the per-TC probability of intensity RI rises substantially, consistent with increased intensity RI observed in other studies (e.g., Bhatia et al., 2018).

3.4. Role of Dry Static Atmospheric Stability

Increased dry static atmospheric stability (DSAS) has been linked to observed decreases in TC near-storm RR (Tu et al., 2021) and RR temporal variability (Deng et al., 2025). Under warming, enhanced upper tropospheric warming relative to lower levels (e.g., Chen & Shi, 2023; Lai & Toumi, 2025) increases DSAS, a trend captured by most climate models despite their projection of increased near-storm RR. In our MRI HighResMIP CMIP6 simulation, DSAS exhibits a significant positive trend over time, with a slope of 0.09 K per year ($p < 0.01, R = 0.975$; Figure 7a). Despite this, near-storm RR and its temporal variability increase. Notably, DSAS shows moderate positive correlations with both near-storm RR RI event ratio ($p < 0.01, R = 0.716$; Figure 7b) and near-storm RR RD event ratio ($p < 0.01, R = 0.691$; Figure 7c). These relationships suggest that

the causal relationship between DSAS and near-storm rainfall dynamics is likely weak or negligible, as local TC dynamics may dominate over large-scale stability influences. While increased DSAS suppresses large-scale circulation, such as the Hadley Circulation, and reduces TC formation, its influence diminishes once a TC forms. Instead of broader dry static stability, local near-storm stability, is more likely relevant to rainfall dynamics. Furthermore, the DSAS metric overlooks the critical role of moisture. In the future warming climate, the increased environmental moisture can destabilize a statically stable atmosphere by lowering the condensation threshold, releasing more latent heat during convection. These processes increase air parcel buoyancy, promoting more vigorous updrafts, leading TC intensity shifting toward higher intensities as evidenced in increasing intense TCs in our climate model (Figures 4a and 4b).

3.5. Discrepancy and Consistency With Observations

The MRI simulations can largely reproduce current rainfall variability. We compared 24-hr near-storm (100 km) ΔR_{24h} from the MRI CMIP6 model (2015–2024) against GPM-derived rainfall observations (2010–2019). The difference in time periods is due to data availability, as the MRI simulation data begins in 2015. The probability density distributions are similar between the MRI model and GPM observation data (see Figure S6 in Supporting Information S1), with the model capturing the 95th percentile of rainfall increases (5.64 mm/hr vs. 5.61 mm/hr in observations) but slightly underestimating rapid decreases (5th percentile: −5.42 mm/hr vs. −6.50 mm/hr). This discrepancy may arise from limitations in model resolution, which can affect the simulation of internal dynamical processes critical for near storm rain rate rapid changes.

Recent observational studies have reported decreased near-storm RR and RR temporal variability in recent decades (Deng et al., 2025; Tu et al., 2021), whereas most model-based studies project increased near-storm RR under warming (Knutson et al., 2020). We found, however, increasing trend in near-storm RR and RR temporal variability under warming. In this study, we do not aim to resolve these discrepancies with recent observations, as short-term trends may be dominated by natural variability, which current GCM resolutions may fail to capture. Instead, we focus on long-term trends under pronounced warming. Despite such discrepancies, a consistent pattern emerges: near-storm rainfall temporal variability is closely tied to near-storm RR itself, with stronger rainfall associated with greater variability. Figure 8 shows interannual trends in near-storm RR relative change (%) and mean RR (mm/h) for RR RI and RD events, where relative change is defined as $\Delta R_{24h}/R_t$ (R_t is the RR at the start of the 24-hr change). For RR RI events, the relative change shows a non-significant trend (slope: −0.04%/year, $p = 0.974$), as does RR RD events (slope: 0.013%/year, $p = 0.51$). However, the annual mean near-storm RR for RI events exhibits a significant increasing trend (slope: 0.028 mm/hr/year, $p < 0.01$), as does RR for RD events (slope: 0.061 mm/hr/year, $p < 0.01$). These findings indicate that the near-storm RR temporal variability, such as RI and RD, may increase or decrease in line with the underlying near-storm RR trend.

3.6. Validation With HighResMIP Simulations

To validate the robustness of the projected increases in near-storm RR variability under future warming, we analyze trends in RR RI and RD event ratios, as well as the relative change in RR for these events, across multiple near-storm radii (100–300 km) and HighResMIP CMIP6 models. This analysis complements the primary findings from the MRI-AGCM3-2-S model by examining results from five additional high-resolution simulations: three ensembles of HadGEM3-GC31-HM (EN1, EN2, EN3) and two of EC-Earth3P-HR (EN1, EN3), all under the SSP5-8.5 scenario. The EN2 ensemble for EC-Earth3P-HR was excluded due to missing data.

Figure 9 presents the regression slopes (%/year) of RR RI and RD event ratios for near-storm rainfall, averaged within radii of 100, 150, 200, and 300 km from TC center, over the period 2015–2050. Across all models and radii, the slopes for both RI and RD event ratios are predominantly positive, with most being statistically significant ($p < 0.05$), indicating a consistent increase in the probability of extreme RR variability events. At the inner 100 km radius, all models exhibit significant positive slopes for RI event ratios, ranging from 0.0399% to 0.1016%/year. For RD event ratios, most models show significant positive slopes, with the notable exception of the MRI model, which displays a non-significant trend (0.0191%/year, $p = 0.3465$). This trend persists at larger radii: at 150 km, RI slopes range from 0.0387% to 0.1117%/year (all $p < 0.05$), and RD slopes from 0.0273% to 0.0877%/year (most $p < 0.05$, except MRI, $p = 0.1273$). At 200 km, HadGEM3-EN1 shows a highly significant RI slope of 0.0609%/year ($p < 0.05$), while EC-Earth3P-HR-EN1 exhibits a strong RD slope of 0.1002%/year

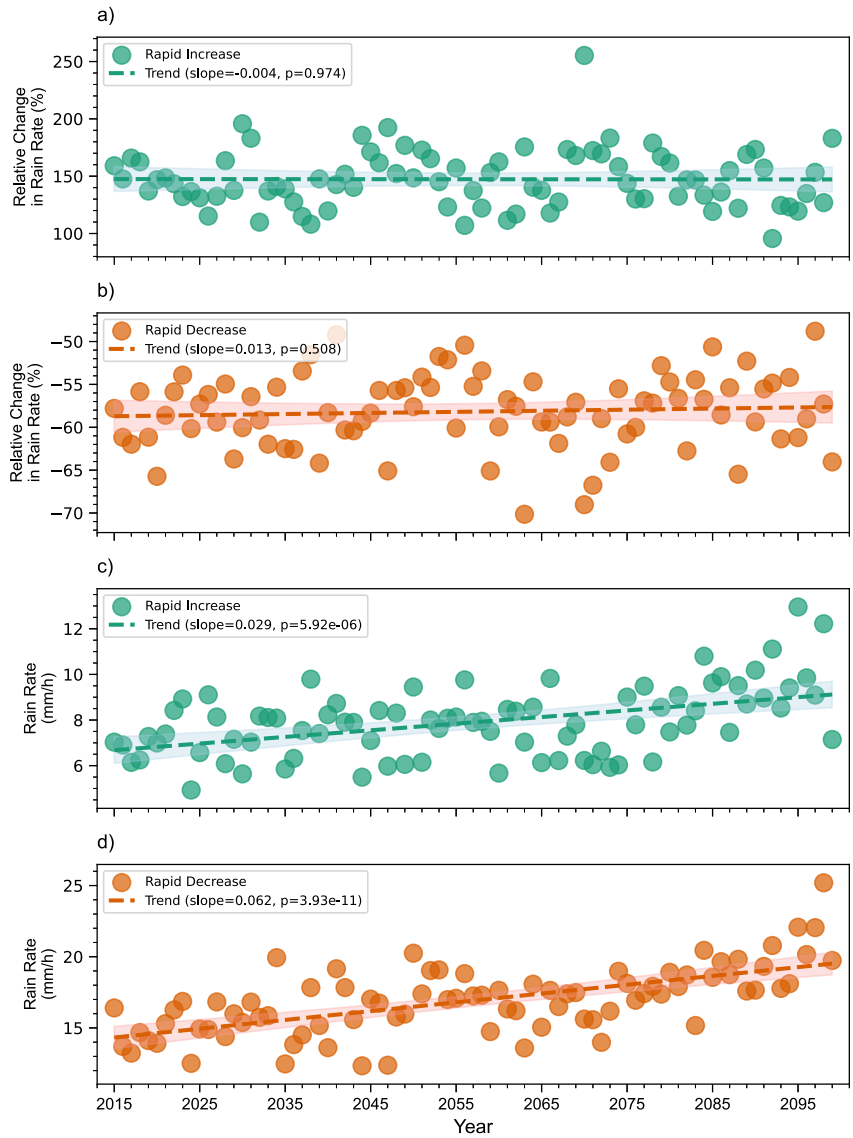

Figure 8. Interannual trends in the near-storm rainfall rate (RR) relative change (%) and near-storm RR (mm/h) for RR rapid increase (RI) events and rapid decrease (RD) events. (a) Mean relative change (%) for RR RI events, calculated as the annual average of $\Delta R_{24h}/R_t$, where R_t is the near-storm RR at the start time of the 24-hr period, with relative changes capped at ±500% and $R_t \geq 0.1$ mm/hr to exclude outliers. (b) Relative change for RR RD events. (c) Annual mean of near-storm RR of RR RI events. (d) Annual mean of near-storm RR of RR RD events. The shaded area indicates the 95% confidence interval for the regression slope.

($p < 0.05$). By 300 km, all simulations maintain significant positive slopes for both RI and RD, reinforcing the consistency across spatial scales.

Figure 10 examines trends in the relative change of RR for RI and RD events, revealing stable relative changes in RR under warming. At the 100 km radius, slopes for RI relative change range from −0.5105% to 0.5312%/year, all non-significant ($p > 0.05$), with similar results for RD events (e.g., MRI: 0.0234%/year, $p = 0.2509$). This lack of significant trends persists across radii, with isolated exceptions such as EC-Earth3P-HR-EN3 showing a significant positive RI slope at 150 km (0.9353%/year, $p = 0.0288$). These cases, however, do not indicate a broader trend, as most slopes remain non-significant (e.g., 300 km, HadGEM3-EN2 RI: 0.5994%/year, $p = 0.0154$, but others $p > 0.05$).

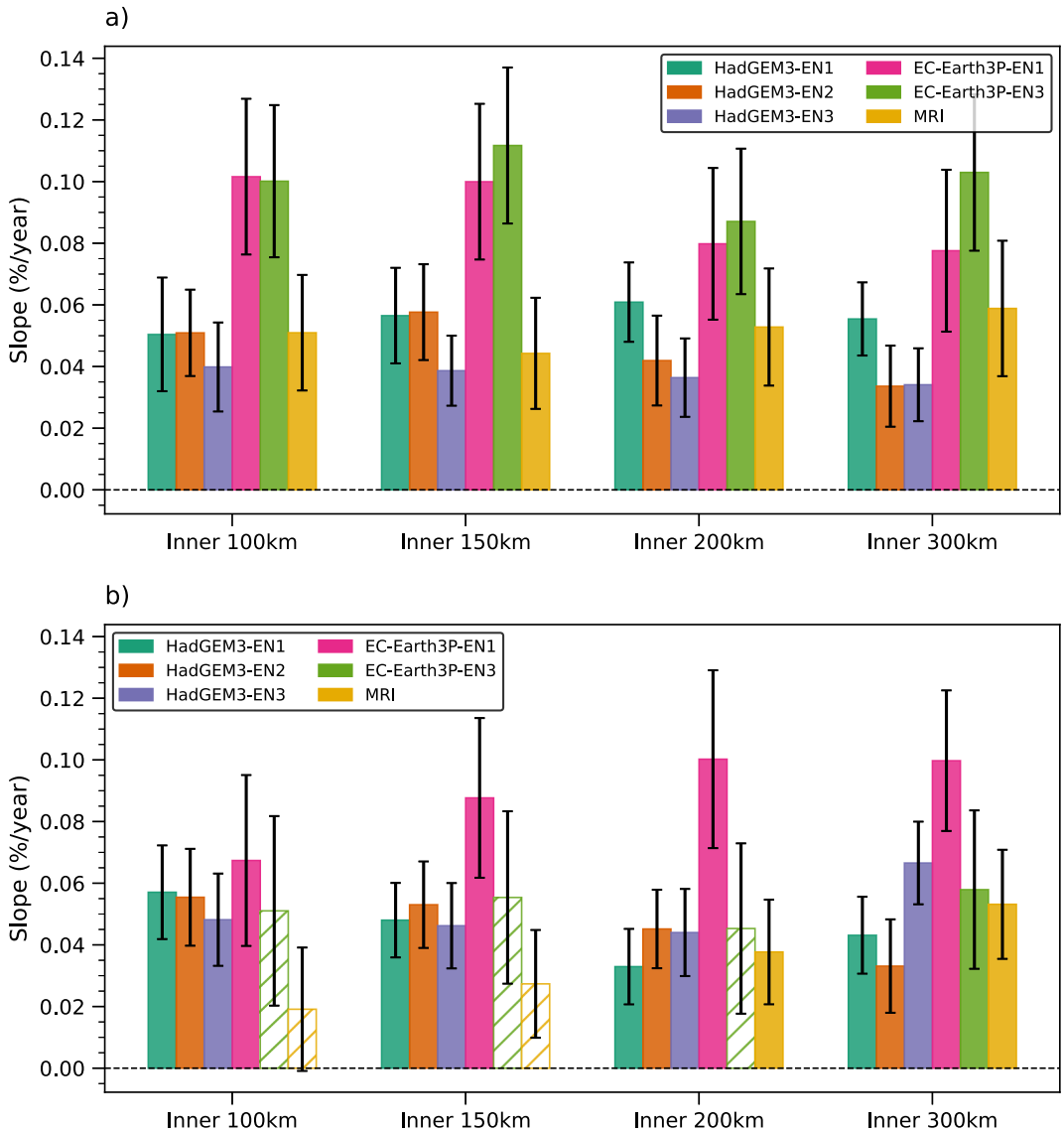

Figure 9. Regression slopes in near-storm rainfall rate rapid increase (a) and rapid decrease (b) event ratios from 2015 to 2050 across multiple climate simulations. Slopes (%/year) for near-storm rainfall using different averaging radii (100, 150, 200, 300 km) from six simulations (HadGEM3-EN1, HadGEM3-EN2, HadGEM3-EN3, EC-Earth3P-HR-EN1, EC-Earth3P-HR-EN3, MRI). Bars represent linear regression slopes with standard error bars. Solid bars indicate statistically significant trends ($p < 0.05$), while hollow bars with hatching indicate non-significant trends.

The robust increase in RI and RD event ratios across simulations, coupled with the lack of consistent trends in relative RR changes, suggests that stronger rainfall intensities under warming are driving greater TC rainfall variability. Notably, the MRI model's non-significant RD event ratio trend at 100 km (0.0191%/year, $p = 0.3465$) in the short-term period (2015–2050) contrasts with its robust, statistically significant increase in RR RD event ratios over the long-term period (2015–2099, slope: 0.041%/year, $p < 0.01$, see Figure 3b). For comparison with the other five simulations, the MRI was analyzed only from 2015 to 2050 to align with their simulation periods, but its long-term results underscore the necessity of extended simulations to confidently identify climate change-driven trends. These findings indicate that increased near-storm RR variability is a robust feature across High-ResMIP CMIP6 models.

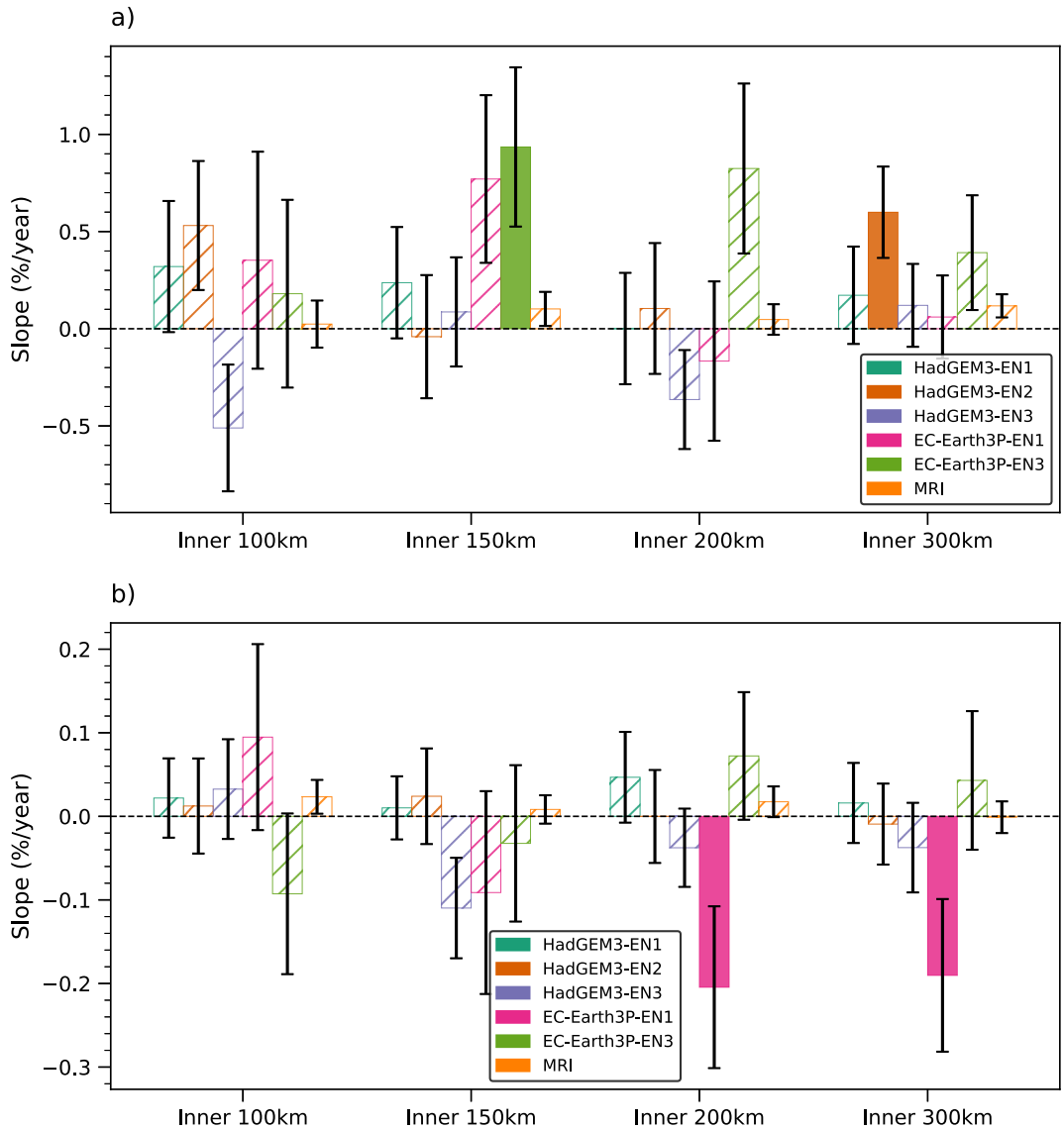

Figure 10. Regression slopes in near-storm rainfall rate relative change (%) from 2015 to 2050 for RR rapid increase (a) and rapid decrease (b) events across multiple climate simulations. Slopes (%/year) for near-storm rainfall using different averaging radii (100, 150, 200, 300 km) from six simulations (HadGEM3-EN1, HadGEM3-EN2, HadGEM3-EN3, EC-Earth3P-HR-EN1, EC-Earth3P-HR-EN3, MRI). Bars represent linear regression slopes with standard error bars. Solid bars indicate statistically significant trends ($p < 0.05$), while hollow bars with hatching indicate non-significant trends.

4. Conclusion

This study uses HighResMIP CMIP6 simulations, primarily the MRI-AGCM3-2-S model (25 km resolution, SSP5-8.5 scenario), to examine the response of tropical cyclone (TC) near-storm rainfall rate (RR) temporal variability to pronounced warming from 2015 to 2099. The MRI data set's high resolution and extended simulation period through 2099 enable improved projections of TC dynamics and detection of long-term climate signals, surpassing the limitations of standard CMIP6 models with typical 100-km resolution. Our findings reveal a significant increase in near-storm RR variability, contrasting with recent observational evidence suggesting decreasing variability over the past two decades (Deng et al., 2025). This discrepancy underscores the need for systematic model-observation comparisons to reconcile differences and the need to understand the influence of natural variability on short-term trends, while our focus on pronounced warming highlights a robust anthropogenic signal in amplifying TC near-storm rainfall variability.

In the MRI simulation, we observe a substantial increase in RR rapid increase (RI) and rapid decrease (RD) events compared to a modest change in TC intensity RI/RD events. Examining the relationship between 24-hr RR changes (ΔR_{24h}, 100-km near-storm) and TC intensity changes (ΔV_{24h}), we find a strong positive correlation, with ΔR_{24h} exhibiting greater sensitivity to ΔV_{24h} in the Future climate. This enhanced sensitivity, along with the pronounced increase in RR RI/RD events, is primarily driven by increased atmospheric moisture, highlighting moisture's dominant role in amplifying rainfall temporal variability under warming. We also reassess the role of dry static atmospheric stability (DSAS) which increases in the future climate. Despite a positive correlation between DSAS and near-storm RR RI/RD ratios, we argue a weak causal link with near-storm rainfall dynamics, as local instability likely plays a more significant role once a TC forms. Under warming, increased DSAS appears to suppress large-scale circulation and TC formation (Sharmila & Walsh, 2018), but its influence on the formed TCs is likely negligible evidenced by TC intensity shifting toward higher intensities in our climate model simulations. Future studies should systematically explore the DSAS–near-storm rainfall relationship to clarify these dynamics.

Validation with five additional HighResMIP CMIP6 simulations confirms consistent increases in RR RI and RD probabilities under warming despite their coarser 50 km resolution and shorter simulation periods. The absence of significant trends in relative RR change ($\Delta R_{24h}/R_t$) across models suggests that absolute rainfall variability scales with near-storm RR trends, linking stronger rainfall intensities to heightened variability.

It is important to emphasize the limitations of this study that we gain the findings of increasing trend of temporal variability of global TC near storm rainfall from HighResCMIP6 simulations. Despite their enhanced resolution compared to standard CMIP6 simulations, these models have critical limitations in resolving fine-scale inner-core rainfall dynamics, such as eyewall structures, inner rainbands, convective bursts, and eyewall replacement cycles. While global cloud-resolving models operating at kilometer scales can effectively capture these dynamics, their substantial computational and storage demands make them impractical for long-term climate projections (Shi et al., 2024), which are central to analyzing temporal rainfall variability. Nevertheless, HighRes CMIP6 simulations remain instrumental in providing first-order estimates of future TC rainfall trends, as demonstrated in numerous studies (e.g., Knutson et al., 2020; Liu et al., 2019; Stansfield & Reed, 2023), offering a foundational perspective on the impacts of global warming on TC behavior.

These findings have profound implications for adaptation planning and risk mitigation in coastal communities. Under warming, TCs will not only produce increased near-storm rainfall but also more frequent RR RI events, causing abrupt downpours that can exceed urban drainage capacities, resulting in flash floods, infrastructure damage and significant economic losses. By leveraging these insights, stakeholders can enhance flood preparedness, strengthen infrastructure resilience, thereby minimizing economic losses and ensuring safety in TC-prone coastal areas.

Conflict of Interest

The authors declare no conflicts of interest relevant to this study.

Data Availability Statement

TempestExtremes software is available at Ullrich et al. (2024). The MRI HighRes CMIP6 data is available at Mizuta et al. (2019). The HadGEM3-GC31-HM data is accessible via M. Roberts (2017). The EC-Earth3P-HR data is accessible via EC-Earth-Consortium (2018).

Acknowledgments
Jianan Chen and Dazhi Xi are supported by an HKU start-up fund 000250348. 130087.25300.100.01. Yanzhen Kang is supported by the Natural Science Foundation of Hunan Province, China (Grant 2025JJ50191) and the Young Scientists Fund of the National Natural Science Foundation of China (Grant 42205007). Ralf Toumi is supported by the Natural Environmental Research Council (NE/W009587/1) and the Singapore Green Finance Centre. Mengqian Lu acknowledges the financial support of the Hong Kong Research Grants Council's general research fund (project no. 16300424) and the support from Otto Poon Centre for Climate Resilience and Sustainability at HKUST. Xiaoming Shi is supported by Grants from the Research Grants Council of the Hong Kong Special Administrative Region, China (project reference numbers AoE/P-601/23-N and HKUST-16307323) and the Center for Ocean Research in Hong Kong and Macau (CORE), which is a joint research center for ocean research between Laoshan Laboratory and HKUST. We also sincerely thank the three anonymous reviewers for their constructive and valuable suggestions, which significantly improved the quality of this manuscript.

References

Bhatia, K., Baker, A., Yang, W., Vecchi, G., Knutson, T., Murakami, H., et al. (2022). A potential explanation for the global increase in tropical cyclone rapid intensification. *Nature Communications*, *13*(1), 6626. https://doi.org/10.1038/s41467-022-34321-6

Bhatia, K., Vecchi, G., Murakami, H., Underwood, S., & Kossin, J. (2018). Projected response of tropical cyclone intensity and intensification in a global climate model. *Journal of Climate*, *31*(20), 8281–8303. https://doi.org/10.1175/JCLI-D-17-0898.1

Bhatia, K., Vecchi, G. A., Knutson, T. R., Murakami, H., Kossin, J., Dixon, K. W., & Whitlock, C. E. (2019). Recent increases in tropical cyclone intensification rates. *Nature Communications*, *10*(1), 635. https://doi.org/10.1038/s41467-019-08471-z

Cao, X., Watanabe, M., Wu, R., Chen, W., Sun, Y., Yan, Q., et al. (2024). The projected poleward shift of tropical cyclogenesis at a global scale under climate change in MRI-AGCM3.2H. *Geophysical Research Letters*, *51*(3), e2023GL107189. https://doi.org/10.1029/2023GL107189

Cao, X., Wu, R., Jiang, X., Dai, Y., Wang, P., Lin, C., et al. (2025). Future changes in tropical cyclone tracks over the Western north Pacific under climate change. *NPJ Climate and Atmospheric Science*, *8*(1), 148. https://doi.org/10.1038/s41612-025-01036-6

Cao, X., Wu, R., Zhu, P., Lan, X., Dai, Y., Bi, M., et al. (2023). Characteristics of barotropic energy conversion in rapid intensifying and decaying tropical cyclones over the Western north Pacific. *Geophysical Research Letters*, *50*(4), e2022GL101695. https://doi.org/10.1029/2022GL101695

Chen, J., & Shi, X. (2023). Quantifying global warming response of the orographic precipitation in a typhoon environment with large-eddy simulations. *Journal of Climate*, *36*(19), 6951–6966. https://doi.org/10.1175/JCLI-D-23-0018.1

Chen, J., Toumi, R., Zhang, L., Lu, M., Xi, D., & Shi, X. (2025). Radial rainfall pattern changes of intense over-ocean tropical cyclones under global warming: Insights from an MRI HighRes CMIP6 simulation. *Geophysical Research Letters*, *52*(9), e2025GL116146. https://doi.org/10.1029/2025GL116146

Deng, E., Xiang, Q., Chan, J. C., Dong, Y., Tu, S., Chan, P.-W., & Ni, Y.-Q. (2025). Increasing temporal stability of global tropical cyclone precipitation. *npj Climate and Atmospheric Science*, *8*(1), 11. https://doi.org/10.1038/s41612-025-00896-2

EC-Earth-Consortium. (2018). Ec-earth-consortium EC-Earth3p-hr model output prepared for CMIP6 HighResMIP [Dataset]. *Earth System Grid Federation*. https://doi.org/10.22033/ESGF/CMIP6.2323

Fischer, M. S., Tang, B. H., & Corbosiero, K. L. (2019). A climatological analysis of tropical cyclone rapid intensification in environments of upper-tropospheric troughs. *Monthly Weather Review*, *147*(10), 3693–3719. https://doi.org/10.1175/mwr-d-19-0013.1

Haarsma, R., Acosta, M., Bakhshi, R., Bretonnière, P.-A., Caron, L.-P., Castrillo, M., et al. (2020). Highresmip versions of Ec-earth: Ec-earth3p and Ec-earth3p-hr–Description, model computational performance and basic validation. *Geoscientific Model Development*, *13*(8), 3507–3527. https://doi.org/10.5194/gmd-13-3507-2020

Huffman, G. J., Stocker, E. F., Bolvin, D. T., Nelkin, E. J., & Tan, J. (2023). GPM IMERG final precipitation L3 half hourly 0.1 degree x 0.1 degree V07. *Data set*. https://doi.org/10.5067/GPM/IMERG/3B-HH/07

Kim, D., Park, D.-S. R., Nam, C. C., & Bell, M. M. (2022). The parametric hurricane rainfall model with moisture and its application to climate change projections. *NPJ Climate and Atmospheric Science*, *5*(1), 86. https://doi.org/10.1038/s41612-022-00308-9

Knutson, T., Camargo, S. J., Chan, J. C. L., Emanuel, K., Ho, C.-H., Kossin, J., et al. (2020). Tropical cyclones and climate change assessment: Part II: Projected response to anthropogenic warming. *Bulletin of the American Meteorological Society*, *101*(3), E303–E322. https://doi.org/10.1175/BAMS-D-18-0194.1

Lai, T.-K., & Toumi, R. (2025). Sensitivity of the energy conversion efficiency of tropical cyclones during intensification to sea surface temperature and static stability. *Quarterly Journal of the Royal Meteorological Society*, *151*(766), e4895. https://doi.org/10.1002/qj.4895

Li, M., & Toumi, R. (2024). On the temporal decay of tropical cyclones over the ocean. *Geophysical Research Letters*, *51*(23), e2024GL111029. https://doi.org/10.1029/2024gl111029

Li, T., Kwon, M., Zhao, M., Kug, J.-S., Luo, J.-J., & Yu, W. (2010). Global warming shifts Pacific tropical cyclone location. *Geophysical Research Letters*, *37*(21), L21804. https://doi.org/10.1029/2010GL045124

Li, Y., Wang, Y., Lin, Y., & Wang, X. (2021). Why does rapid contraction of the radius of maximum wind precede rapid intensification in tropical cyclones? *Journal of the Atmospheric Sciences*, *78*(11), 3441–3453. https://doi.org/10.1175/jas-d-21-0129.1

Liu, M., Vecchi, G. A., Smith, J. A., & Knutson, T. R. (2019). Causes of large projected increases in hurricane precipitation rates with global warming. *NPJ Climate and Atmospheric Science*, *2*(1), 38. https://doi.org/10.1038/s41612-019-0095-3

Lockwood, J. W., Lin, N., Gori, A., & Oppenheimer, M. (2024). Increasing flood hazard posed by tropical cyclone rapid intensification in a changing climate. *Geophysical Research Letters*, *51*(5), e2023GL105624. https://doi.org/10.1029/2023GL105624

Ma, Z., Fei, J., & Huang, X. (2019). A definition of rapid weakening for tropical cyclones over the Western north Pacific. *Geophysical Research Letters*, *46*(20), 11471–11478. https://doi.org/10.1029/2019gl085090

Mizuta, R., Yoshimura, H., Ose, T., Hosaka, M., & Yukimoto, S. (2019). MRI MRI-AGCM3-2-S model output prepared for CMIP6 HighResMIP highressst-future [Dataset]. *Earth System Grid Federation*. https://doi.org/10.22033/ESGF/CMIP6.6740

Patricola, C. M., & Wehner, M. F. (2018). Anthropogenic influences on major tropical cyclone events. *Nature*, *563*(7731), 339–346. https://doi.org/10.1038/s41586-018-0673-2

Roberts. (2019). CMIP6 HighResMIP: Tropical storm tracks as calculated by the TempestExtremes algorithm. Retrieved from http://catalogue.ceda.ac.uk/uuid/438268b75fed4f27988dc02f8a1d756d

Roberts. (2019). CMIP6 HighResMIP: Tropical storm tracks as calculated by the TRACK algorithm. Retrieved from http://catalogue.ceda.ac.uk/uuid/0b42715a7a804290afa9b7e31f5d7753

Roberts, J., Camp, J., Seddon, J., Vidale, P. L., Hodges, K., et al. (2020). Projected future changes in tropical cyclones using the CMIP6 HighResMIP multimodel ensemble. *Geophysical Research Letters*, *12*, e2020GL088662. https://doi.org/10.1029/2020GL088662

Roberts, M. (2017). Mohc hadgem3-gc31-hm model output prepared for cmip6 highresmip [Dataset]. *Earth System Grid Federation*. https://doi.org/10.22033/ESGF/CMIP6.446

Roberts, Baker, A., Blockley, E. W., Calvert, D., Coward, A., Hewitt, H. T., et al. (2019). Description of the resolution hierarchy of the global coupled hadgem3-gc3.1 model as used in cmip6 highresmip experiments. Geosci. *Model Dev.*, *12*, 4999–5028. https://doi.org/10.5194/gmd-12-4999-2019

Sharmila, S., & Walsh, K. J. (2018). Recent poleward shift of tropical cyclone formation linked to hadley cell expansion. *Nature Climate Change*, *8*(8), 730–736. https://doi.org/10.1038/s41558-018-0227-5

Shi, X., Liu, Y., Chen, J., Chen, H., Wang, Y., Lu, Z., et al. (2024). Escalating tropical cyclone precipitation extremes and landslide hazards in south China under global warming. *npj Climate and Atmospheric Science*, *7*(1), 107. https://doi.org/10.1038/s41612-024-00654-w

Stansfield, A. M., & Rasmussen, K. L. (2025). The response of tropical cyclone inner core and outer rainband precipitation to warming in idealized convection-permitting WRF. *Journal of Geophysical Research: Atmospheres*, *130*(4), e2024JD042217. https://doi.org/10.1029/2024JD042217

Stansfield, A. M., & Reed, K. A. (2023). Global tropical cyclone precipitation scaling with sea surface temperature. *npj Climate and Atmospheric Science*, *6*(1), 60. https://doi.org/10.1038/s41612-023-00391-6

Tu, S., Xu, J., Chan, J. C. L., Huang, K., Xu, F., & Chiu, L. S. (2021). Recent global decrease in the inner-core rain rate of tropical cyclones. *Nature Communications*, *12*(1), 1948. https://doi.org/10.1038/s41467-021-22304-y

Ullrich, P., Zarzycki, C. M., McClenny, E. E., Pinheiro, M. C., Stansfield, A. M., & Reed, K. A. (2021). TempestExtremes v2.1: A community framework for feature detection, tracking, and analysis in large datasets. *Geoscientific Model Development*, *14*(8), 5023–5048. https://doi.org/10.5194/gmd-14-5023-2021

Ullrich, P., Zarzycki, C. M., McClenny, E. E., Pinheiro, M. C., Stansfield, A. M., & Reed, K. A. (2024). Tempestextremes [Software]. Retrieved from https://github.com/ClimateGlobalChange/tempestextremes

Wang, S., Rashid, T., Throp, H., & Toumi, R. (2020). A shortening of the life cycle of major tropical cyclones. *Geophysical Research Letters*, *47*(14), e2020GL088589. https://doi.org/10.1029/2020GL088589

Wang, X., & Jiang, H. (2021). Contrasting behaviors between the rapidly intensifying and slowly intensifying tropical cyclones in the north Atlantic and eastern Pacific basins. *Journal of Climate*, *34*(3), 987–1003. https://doi.org/10.1175/jcli-d-19-0908.1

Xi, D., Wang, S., & Lin, N. (2022). Analyzing relationships between tropical cyclone intensity and rain rate over the ocean using numerical simulations. *Journal of Climate*, *36*, 1–24. https://doi.org/10.1175/JCLI-D-22-0141.1

Yang, Y., & Toumi, R. (2025). Large dynamic contributions to tropical cyclone precipitation with increasing sea surface temperature. *Environmental Research Letters*, *20*(7), 074013. https://doi.org/10.1088/1748-9326/add753